

A Moment Matching-Based Method for Sparse and Noisy Point Cloud Registration

Xingyi Li, Han Zhang, Ziliang Wang, Yukai Yang, Weidong Chen

Abstract—Point cloud registration is a key step in robotic perception tasks, such as Simultaneous Localization and Mapping (SLAM). It is especially challenging in conditions with sparse points and heavy noise. Traditional registration methods, such as Iterative Closest Point (ICP) and Normal Distributions Transform (NDT), often have difficulties in achieving a robust and accurate alignment under these conditions. In this paper, we propose a registration framework based on moment matching. In particular, the point clouds are regarded as i.i.d. samples drawn from the same distribution observed in the source and target frames. We then match the generalized Gaussian Radial Basis moments calculated from the point clouds to estimate the rigid transformation between two frames. Moreover, such method does not require explicit point-to-point correspondences among the point clouds. We further show the consistency of the proposed method. Experiments on synthetic and real-world datasets show that our approach achieves higher accuracy and robustness than existing methods. In addition, we integrate our framework into a 4D Radar SLAM system. The proposed method significantly improves the localization performance and achieves results comparable to LiDAR-based systems. These findings demonstrate the potential of moment matching technique for robust point cloud registration in sparse and noisy scenarios.

I. INTRODUCTION

With the increasing availability of 3D scanning devices like LiDAR and 4D radar sensors, point clouds have become a common representation for capturing real-world geometry. A fundamental task in processing point clouds is registration. Point cloud registration has been widely used in applications like robotic perception and autonomous driving [1]. More specifically, registration is the process of estimating the transformation between multiple point sets and aligning them into a unified coordinate frame.

Among the widely used methods for point cloud registration, there are two most popular methods: Iterative Closest Point (ICP) [2] and Normal Distributions Transform (NDT) [3], [4]. In particular, ICP operates by iteratively minimizing the distance between closest points of two point clouds. In contrast, NDT first estimates the distribution of one point cloud with a Gaussian mixture distribution over a voxelized grid. Then, the other cloud is registered by maximizing the likelihood of its points under this estimated distribution. However, both methods have their own limitations, particularly when dealing with sparse and noisy data. On the one hand, for ICP and other ICP-variants methods, severe noise and outliers in sensor measurements will reduce reliable correspondences and lead to unstable convergence. On the other hand, the performance of NDT heavily depends on the voxel size selection. And in very sparse point clouds, the statistical estimation of mixed Gaussian distribution becomes

unreliable. This is because of the following dilemma: to approximate the whole object distribution in the environment with Gaussian mixture, it is preferable to have a finer voxel resolution. However, the smaller voxel grid size leads to the point cloud insufficiency in each grid, and the mean and the covariance estimation in each voxel grid becomes inaccurate.

To address these limitations, in this paper, we propose Moment Matching Registration (MMR), a moment matching-based registration framework without requiring point correspondences or local density estimation. In particular, we regard the point clouds as i.i.d. samples drawn from the same objects distribution of the environment observed in both source and target frame. We then match the generalized moments calculated from the point clouds, and find the rigid transformation between the frames. More specifically, the k -th order generalized moments of the object distribution μ takes the form

$$m_k^\mu = \mathbb{E}_\mu[\phi_k] = \int \phi_k(\mathbf{x})\mu(d\mathbf{x}) \approx \frac{1}{N} \sum_{i=1}^N \phi_k(x_i) := \hat{m}_k(\mathcal{X}),$$

where N is the point cloud size, ϕ_k is some kernel function, $x_i \in \mathcal{X}$ is the coordinate of the i -th point from point cloud \mathcal{X} , and is i.i.d. sampled from μ . With properly selected kernel functions, the generalized moments $\{m_k\}_{k=1}^\infty$ should carry the overall information of the distribution μ [5]. More specifically, we choose Gaussian Radial Basis Function (RBF) kernel to construct the generalized moments in this paper. Such method is free of point correspondence and remains robust and accurate in sparse and noisy scenarios. Moreover, the summation structure in generalized moment approximation makes it easy to leverage CUDA parallelization and achieve computational efficiency for real-time applications.

The main contribution of our work is three-fold:

- First, we propose a point cloud registration framework. It leverages moment matching to align the object distributions observed in the source and target frames and estimate the transformation between the frames. It does not rely on explicit correspondences between the points.
- Second, we prove the proposed registration algorithm is statistically consistent, that is, the transformation estimation converges in probability to the “true” transformation as the number of the points in the point cloud goes to infinity. This is the first robust guarantee of the algorithm against noise when the numbers of points in clouds are relatively sufficient.
- Experiments on both synthetic and real-world datasets have been conducted to test the method’s performance.

Consequently, we outperform other commonly used methods such as GICP and NDT, especially in challenging scenarios with low point density and high noise.

II. RELATED WORK

A. Conventional registration methods

Conventional point cloud registration methods aim to find the best transformation that aligns two sets of 3D points. The most widely used approach is the Iterative Closest Point (ICP) algorithm [2]. ICP works by repeatedly finding the nearest neighbors between two point clouds and computing a transformation to minimize the distance between them. ICP is simple and effective when the point clouds are clean and roughly aligned, but it performs poorly when the data is noisy, sparse, or when the initial alignment is not good.

To improve ICP, Generalized ICP (GICP) [6] combines point-to-point and point-to-plane constraints, which gives better results on surfaces and structured scenes. Voxelized GICP (VGICP) [7] further improves efficiency by using voxel grids to reduce the number of points and smooth the data. These methods offer better accuracy and speed, but they still depend on good initial alignment and can fail in low-overlap or high-noise situations.

Another well-known method is the Normal Distributions Transform (NDT) [4], which represents the target point cloud as a set of Gaussian distributions inside a voxel grid. The source points are aligned by maximizing their likelihood under this model. NDT works better than ICP in many real-world applications, especially with dense LiDAR data. However, NDT depends heavily on the size of the voxels, and it does not work well when the point cloud is very sparse or unevenly distributed.

B. Feature-based registration methods

Feature-based methods extract keypoints and descriptors from the point cloud to match corresponding parts of two shapes. These methods are less sensitive to noise and partial overlap because they do not require matching every point.

One commonly used local descriptor is FPFH (Fast Point Feature Histogram) [8], which captures the geometric relationships between a point and its neighbors. It is fast and widely used for coarse alignment. However, FPFH is sensitive to noise and not very discriminative in flat areas.

Another popular descriptor is SHOT (Signature of Histograms of Orientations) [9], which is more robust to rotation and captures more detailed local geometry. SHOT performs better than FPFH in complex scenes, but it is also more computationally expensive.

These feature-based methods work well when the points have rich geometric structure and sufficient resolution. However, when the data is very sparse, noisy, or lacks strong features, these descriptors may fail to produce reliable matches.

C. Learning-based registration methods

Deep learning has recently been applied to point cloud registration to improve robustness and remove the need for

hand-crafted features. These methods use neural networks to learn features and matching strategies directly from data.

DCP (Deep Closest Point) [10] introduces an attention mechanism to learn soft correspondences between point clouds. It performs well under low-overlap conditions. However, DCP may not generalize well to new data and its dependence on dense and reliable feature matches results in degraded alignment under sparse or noisy conditions.

In addition, PointNetLK [11] combines the PointNet [12] architecture with a classical Lucas-Kanade optimization process. It learns global features and updates the transformation iteratively without requiring explicit correspondences. However, the use of a numerical Jacobian leads to instability and poor generalization. To address these limitations, PointNetLK Revisited [13] replaces the numerical Jacobian with an analytical decomposition, improving stability and allowing better feature reuse. Nevertheless, it still depends on supervised training with large datasets and its performance degrades when facing unseen environments.

In summary, conventional methods like ICP, NDT and their extensions are simple and fast, but not robust to sparse or noisy data. Feature-based methods work better in structured scenes but often fail when features are weak. Learning-based methods show strong results, but they rely on large-scale supervised training and may not generalize well to unseen sensor modalities or environments. Consequently, we aim to develop a training-free, and robust registration method in sparse and noisy conditions. And we will introduce the method in detail in the next section. Moreover, to be fair, the comparisons in Sec. IV will be focused on classical registration algorithms that share the same deployment constraints as our proposed method.

III. METHODOLOGY

In this section, we introduce our point cloud registration method using moment matching. This section is organized as follows: First, we introduce the notations and basic setup used throughout the paper. Then, we explain how to compute moments with Gaussian RBF to represent the distribution of a point cloud. Next, we present the optimization process to estimate the transformation which aligns point clouds by minimizing the difference between their moments. Finally, we introduce a CUDA-based parallelization method to accelerate the computation of moment matching, enabling real-time performance of our framework.

A. Notations and Preliminaries

Consider a static environment containing multiple objects. A sensor captures this scene from two different viewpoints, referred to as the source frame and the target frame. Consequently, two point clouds are obtained by sampling from the same surface represented in different coordinate systems.

To formulate this, let $(\mathbb{R}^3, \mathcal{B}(\mathbb{R}^3), \mu)$ be the probability space carried by the target frame, where $\mathcal{B}(\mathbb{R}^3)$ is the Borel σ -algebra in \mathbb{R}^3 , and μ is the probability measure such that $\mu(A)$ is the probability that the point cloud lies in $A \subset \mathbb{R}^3$ in the target frame. And the support of μ is $\text{supp}(\mu) := \mathbb{K}$.

Moreover, let $(\mathbb{R}^3, \mathcal{B}(\mathbb{R}^3))$ be the measurable space in the source frame. Furthermore, let $T : \mathbb{R}^3 \times \text{SE}(3) \rightarrow \mathbb{R}^3$ be the rigid transformation, i.e., for $\mathbf{x} \in \mathbb{R}^3$ in the source frame and $\mathbf{y} \in \mathbb{R}^3$ in the target frame,

$$\mathbf{y} = T(\mathbf{x}; \underbrace{(\mathbf{R}, \mathbf{t})}_{\theta}) = \mathbf{R}\mathbf{x} + \mathbf{t},$$

where $(\mathbf{R}, \mathbf{t}) \in \text{SE}(3)$, $\mathbf{R} \in \text{SO}(3)$ is a rotation matrix and $\mathbf{t} \in \mathbb{R}^3$ is a translation vector. The “true” rigid transformation that transforms the source to the target frame is denoted as $T_0 := T(\cdot; \theta_0)$, where $\theta_0 := (\mathbf{R}_0, \mathbf{t}_0)$ is the “true” rotation matrix and translation vector. Clearly, $T(\cdot; \theta)$ is a measurable function for all $\theta \in \text{SE}(3)$ and we denote $\mu \circ T_0$ as the probability measure induced by $T(\cdot; \theta_0)$. In particular, for any $B \subseteq \mathbb{R}^3$, it holds that $(\mu \circ T_0)(B) := \mu(T(B; \theta_0))$, where $T(B; \theta_0)$ is the image of B under T_0 . Consequently, we model the point clouds \mathcal{X} and \mathcal{Y} observed in the source and target frames, respectively, as

- $\mathcal{Y} = \{y_j \in \mathbb{R}^3\}_{j=1}^M$, where y_j is the realization of the random vector $\mathbf{y}_j \stackrel{\text{i.i.d.}}{\sim} \mu$;
- $\mathcal{X} = \{x_i \in \mathbb{R}^3\}_{i=1}^N$, where x_i is the realization of the random vector $\mathbf{x}_i \stackrel{\text{i.i.d.}}{\sim} \mu \circ T_0$.

Equipped with the above formulation, we aim to estimate the “true” parameter θ_0 that defines the “true” rigid transformation T_0 with the point clouds \mathcal{X} and \mathcal{Y} .

B. The Generalized Moments and its approximations

To register the point clouds and estimate θ_0 , we need to compare and match the “features” of the distributions μ and $\mu \circ T_0$. To this end, we choose to match the generalized moments of μ and $\mu \circ T_0$. In general, a moment can be defined as the expectation of a measurable function with respect to a probability or finite measure. More specifically, let ν be a nonnegative Borel measure defined on $\text{supp}(\nu) := \mathbb{K} \subseteq \mathbb{R}^d$, and let $\phi_k : \mathbb{R}^d \rightarrow \mathbb{R}$ be a measurable kernel function. The k -th moment with respect to ν is defined as

$$m_k^\nu = \int_{\mathbb{K}} \phi_k(\mathbf{x}) \nu(d\mathbf{x}).$$

This formulation includes classical monomial moments (i.e., $\phi_k(\mathbf{x}) = x^{k_x} y^{k_y} z^{k_z}$, where $\mathbf{x} = [x, y, z]^T$ and $k_x + k_y + k_z = k$) as well as more general moments constructed from non-monomial functions. When ν is a probability measure, this reduces to expectation $m_k^\nu = \mathbb{E}_\nu[\phi_k(\mathbf{x})]$.

In the case of point cloud registration, we do not know the explicit distribution μ . Hence, it is difficult to calculate the generalized moments explicitly. Nevertheless, since the point clouds \mathcal{X} and \mathcal{Y} are i.i.d. sampled from the probability measures $\mu \circ T$ and μ , we approximate the expectations using empirical averages. More specifically, the empirical k -th moment of the target point cloud \mathcal{Y} takes the form

$$m_k^\mu = \mathbb{E}_\mu[\phi_k(\mathbf{y})] \approx \frac{1}{M} \sum_{j=1}^M \phi_k(\mathbf{y}_j) := \hat{m}_k(\mathcal{Y}). \quad (1)$$

Moreover, by applying the change of variable $\mathbf{y} = T(\mathbf{x}; \theta_0)$, it also holds for the generalized moment m_k^μ in (1) that

$$\begin{aligned} m_k^\mu &= \int_{\mathbb{K}} \phi_k(\mathbf{y}) \mu(d\mathbf{y}) = \int_{\mathbb{K}} \phi_k(T(\mathbf{x}; \theta_0)) \mu(dT(\mathbf{x}; \theta_0)) \\ &= \int_{T_0^{-1}(\mathbb{K})} \phi_k(T(\mathbf{x}; \theta_0)) (\mu \circ T_0)(d\mathbf{x}) = \mathbb{E}_{\mu \circ T_0}[\phi_k(T(\mathbf{x}; \theta_0))] \\ &\approx \frac{1}{N} \sum_{i=1}^N \phi_k(T(\mathbf{x}_i; \theta_0)) := \hat{m}_k(T(\mathcal{X}; \theta_0)). \end{aligned} \quad (2)$$

The empirical moments serve as a concise approximation of the point cloud distribution “features”. As we shall see in Sec. III-D, we will minimize the difference between the empirical moments with respect to θ to estimate the “true” rigid transformation θ_0 .

C. Kernel Function Design

The choice of kernel function ϕ_k plays an important role and it affects the sensitivity and robustness of the final registration result. In this work, we adopt the Gaussian Radial Basis Function (RBF) as our kernel function, given by,

$$\phi_k(\mathbf{x}) = e^{-(\mathbf{x} - \mathbf{c}_k)^\top \Sigma^{-1} (\mathbf{x} - \mathbf{c}_k)}, \quad (3)$$

where $\mathbf{c}_k \in \mathbb{R}^3$ is the center of the kernel, and Σ determines the width of the “Gaussian bell”. Intuitively speaking, each generalized moment with the kernel (3) captures the local features of the distributions μ around the center \mathbf{c}_k , since the value of $\phi_k(\mathbf{x})$ decays exponentially fast as \mathbf{x} leaves the center \mathbf{c}_k . And by placing the centers $\mathcal{P}_c := \{\mathbf{c}_k\}_{k=1}^\kappa$ in the 3D space of point cloud, we can capture the global “features” in the points distribution.

Next, we shall choose the centers $\mathcal{P}_c := \{\mathbf{c}_k\}_{k=1}^\kappa$ and Σ to ensure the effectiveness and efficiency of such “feature capture”. To this end, we adopt an adaptive strategy for selecting the centers of the Gaussian RBF kernels based on the density of the input point cloud. More specifically, if the point cloud is sparse or contains points fewer than a predefined threshold, then each point will serve as a center. This ensures a more effective “feature capture” using the generalized Gaussian RBF moments – if the centers are not placed carefully when the point clouds are sparse, then most of the empirical Gaussian RBF moments would be almost zero. On the other hand, for denser point clouds, we apply k -means clustering to select a compact set of representative centers. This ensures that the centers are placed at where the points are dense to extract local “features” of the point cloud distribution, while keeping a reasonable number of centers (order of moments) so that we can have a tolerable computational cost. After we choose the centers $\mathcal{P}_c := \{\mathbf{c}_k\}_{k=1}^\kappa$, the parameter Σ is determined empirically in our experiments.

D. Transformation Estimation

We now start to construct the optimization problem that matches the moments and estimate the “true” rigid transformation θ_0 . Note that as expressed in (1) and (2), both $\mathbb{E}_\mu[\phi_k(\mathbf{y})]$ and $\mathbb{E}_{\mu \circ T_0}[\phi_k(T(\mathbf{x}; \theta_0))]$ equal to m_k^μ . Hence,

the two empirical approximations $\hat{m}_k(\mathcal{Y})$ and $\hat{m}_k(T(\mathcal{X}; \theta_0))$ should coincide since they both approximate the same m_k^μ . Therefore, we can estimate the optimal transformation by minimizing the difference between the empirical moments of the transformed source and those of the target with respect to the parameter θ . In particular, we use the least-square loss

$$\begin{aligned} \mathcal{L}(\theta) &= \sum_{k=1}^{\kappa} \|\mathbb{E}_{\mu \circ T}[\phi_k(T(\mathbf{x}; \theta))] - \mathbb{E}_{\mu}[\phi_k(\mathbf{y})]\|^2 \\ &\approx \sum_{k=1}^{\kappa} \|\hat{m}_k(T(\mathcal{X}; \theta)) - \hat{m}_k(\mathcal{Y})\|^2 := \mathcal{L}_{M,N}(\theta), \end{aligned} \quad (4)$$

where $\hat{m}_k(\cdot)$ denotes the k -th order empirical moment of order k . By substituting the expressions (1), (2) and (3) into (4), we obtain the optimization that we actually solve to estimate the rigid transformation θ_0

$$\begin{aligned} \min_{\theta \in \mathcal{B}(\eta)} \mathcal{L}_{M,N}(\theta) &= \sum_{k=1}^{\kappa} \left[\frac{1}{N} \sum_{i=1}^N e^{-(\mathbf{R}\mathbf{x}_i + \mathbf{t} - \mathbf{c}_k)^\top \Sigma^{-1} (\mathbf{R}\mathbf{x}_i + \mathbf{t} - \mathbf{c}_k)} \right. \\ &\quad \left. - \frac{1}{M} \sum_{j=1}^M e^{-(\mathbf{y}_j - \mathbf{c}_k)^\top \Sigma^{-1} (\mathbf{y}_j - \mathbf{c}_k)} \right]^2, \end{aligned} \quad (5)$$

where $\mathcal{B}(\eta) := \{\theta \mid (\mathbf{R}, \mathbf{t}) \in \text{SE}(3), \|\mathbf{t}\|^2 \leq \eta\}$ is the compact feasible domain for θ , and η is a pre-defined constant that can be arbitrarily large.

Suppose $\hat{\theta}_{M,N}$ is the minimizer of (5), we would like to state the consistency of such estimate, which we refer to the following theorem. This is the first robust guarantee of the algorithm against noise when the numbers of points in clouds are relatively sufficient.

Theorem 1 (Statistical consistency of the estimator):

Suppose that the centers $\{\mathbf{c}_k\}_{k=1}^{\kappa}$ do not lie in any hyperplane in \mathbb{R}^3 . Then, the estimator $\hat{\theta}_{M,N} \xrightarrow{P} \theta_0$ as $M \rightarrow \infty$ and $N \rightarrow \infty$.

Proof: See Appendix. ■

Our objective function $\mathcal{L}_{M,N}(\theta)$ is differentiable with respect to the parameter θ . To efficiently minimize $\mathcal{L}_{M,N}(\theta)$, we employ the Broyden-Fletcher-Goldfarb-Shanno (BFGS) quasi-Newton method [14], [15]. Moreover, we parameterize the rotation matrix $\mathbf{R} \in \text{SO}(3)$ with Euler angles. Such parameterization transforms the optimization problem from matrix space into vector space, making it more tractable for quasi-Newton methods. In addition, the expression of gradient $\frac{\partial \mathcal{L}_{M,N}(\theta)}{\partial \theta}$ is pre-computed via chain rule. That is, the derivative of the empirical moment terms with respect to the Euler angles ψ_i takes the form $\frac{\partial \hat{m}_k(T(\mathcal{X}; \theta))}{\partial \psi_i} = \frac{\partial \hat{m}_k(T(\mathcal{X}; \theta))}{\partial \mathbf{R}} \frac{\partial \mathbf{R}}{\partial \psi_i}$. In summary, the transformation estimation process is shown in Algorithm 1.

The proposed method is inherently robust to both noise and sparsity. In particular, since the effect of the potential measurement noise is intrinsically included in the point distributions, and the registration is based on the statistical properties of the distribution instead of any specific structural features like “lines”, “planes” or “the nearest neighbor”, etc., the method is intrinsically robust to noisy point clouds.

Algorithm 1: Moment Matching Registration

Input: Source point cloud \mathcal{X} , Target point cloud \mathcal{Y}

Output: The estimate $\hat{\theta}_{M,N}$ of the optimal rigid transformation parameter θ_0 .

Initialization:

Allocate center points $\mathcal{P}_c := \{\mathbf{c}_k\}_{k=1}^{\kappa}$

forall center $\mathbf{c}_k \in \mathcal{P}_c$ **do in parallel**

foreach point $\mathbf{y}_j \in \mathcal{Y}$ **do**

 | Compute $\phi_k(\mathbf{y}_j)$

end

$\hat{m}_k(\mathcal{Y}) \leftarrow \frac{1}{M} \sum_{i=1}^N \phi_k(\mathbf{y}_j)$

end

Registration:

while not converged do

$\mathcal{L}_{M,N}(\theta) \leftarrow 0$

 Initialize transformation $T(\cdot; \theta)$

forall center $\mathbf{c}_k \in \mathcal{P}_c$ **do in parallel**

foreach point $\mathbf{x}_i \in \mathcal{X}$ **do**

 | Compute $\phi_k(T(\mathbf{x}_i; \theta))$

end

$\hat{m}_k(T(\mathcal{X}; \theta)) \leftarrow \frac{1}{N} \sum_{i=1}^N \phi_k(T(\mathbf{x}_i; \theta))$

$\Delta_k(\theta) \leftarrow (\hat{m}_k(T(\mathcal{X}; \theta)) - \hat{m}_k(\mathcal{Y}))^2$

 Compute gradient $\nabla_{\theta} \Delta_k(\theta)$

end

$\mathcal{L}_{M,N}(\theta) \leftarrow \sum_{k=1}^{\kappa} \Delta_k(\theta)$

$\nabla_{\theta} \mathcal{L}_{M,N}(\theta) \leftarrow \sum_{k=1}^{\kappa} \nabla_{\theta} \Delta_k(\theta)$

 Update θ using BFGS method

end

return $\hat{\theta}_{M,N}$

Moreover, the choice of Gaussian RBF makes the contribution of outliers to the moments extremely small due to the exponential decay of kernel function. Hence our method also reduces the sensitivity to outliers. For sparse points, our method avoids reliance on local statistics, which typically requires a sufficient number of points within voxel grids to obtain accurate approximations of the statistics such as mean and covariance as in NDT. The proposed method utilizes generalized moments that is based on the entire point cloud, enabling a robust registration for sparse point clouds.

To further enhance computational efficiency, we implement the moment computations and transformation updates using CUDA parallelization, as detailed in next section.

E. CUDA Acceleration

In order to improve the computational efficiency of our moment matching registration framework, we implement key components of the algorithm using CUDA-based parallel computing on GPU for acceleration.

In particular, the most computationally intensive parts of our method involve

- Computing the Gaussian RBF kernel values $\phi_k(\cdot)$ for all points and centers.
- Evaluating the moment matching loss $\mathcal{L}_{M,N}(\theta)$ and its gradient $\nabla_{\theta} \mathcal{L}_{M,N}$ during optimization.

TABLE I: Translation and rotation error (m / deg) on noiseless point clouds.

Method	Bunny	Dragon	Buddha	Armadillo
GICP [6]	$3.38 \times 10^{-3} / 2.39 \times 10^{-2}$	$6.91 \times 10^{-2} / 0.49$	$9.12 \times 10^{-3} / 9.83 \times 10^{-2}$	$7.43 \times 10^{-4} / 3.88 \times 10^{-3}$
NDT [4]	$4.75 \times 10^{-3} / 2.74 \times 10^{-2}$	$1.03 \times 10^{-2} / 6.89 \times 10^{-2}$	$4.17 \times 10^{-3} / 2.15 \times 10^{-2}$	$3.79 \times 10^{-3} / 2.04 \times 10^{-2}$
Ours	$5.50 \times 10^{-8} / 1.15 \times 10^{-15}$	$6.52 \times 10^{-7} / 1.16 \times 10^{-15}$	$1.00 \times 10^{-8} / 1.15 \times 10^{-15}$	$3.89 \times 10^{-8} / 1.15 \times 10^{-15}$

TABLE II: Translation and rotation error (m / deg) on noisy point clouds.

Method	Noisy Bunny	Noisy Dragon	Noisy Buddha	Noisy Armadillo
GICP [6]	$1.59 \times 10^{-2} / 0.14$	$0.11 / 0.53$	$2.92 \times 10^{-2} / 0.15$	$4.48 \times 10^{-2} / 0.24$
NDT [4]	$5.63 \times 10^{-3} / 4.38 \times 10^{-2}$	$3.89 \times 10^{-3} / 1.54 \times 10^{-2}$	$9.24 \times 10^{-3} / 6.38 \times 10^{-2}$	$3.33 \times 10^{-3} / 1.71 \times 10^{-2}$
Ours	$1.90 \times 10^{-3} / 2.10 \times 10^{-2}$	$3.06 \times 10^{-3} / 9.98 \times 10^{-3}$	$4.63 \times 10^{-3} / 3.12 \times 10^{-2}$	$1.68 \times 10^{-3} / 1.21 \times 10^{-2}$

TABLE III: Comparison of the relative and absolute errors (% / deg/m / m) in different real-world scenes.

SLAM Method	Campus 1	Campus 2	Campus 3
LiDAR SLAM [16], [17]	1.96 / 0.0209 / 2.27	3.19 / 0.0120 / 2.57	2.68 / 0.0173 / 3.33
4DRaSLAM [18]	2.32 / 0.0216 / 2.28	3.13 / 0.0201 / 3.79	3.06 / 0.0245 / 3.83
Ours	2.02 / 0.0169 / 2.11	2.75 / 0.0137 / 6.60	2.70 / 0.0160 / 3.46

By leveraging the parallel computing on GPUs, we assign each CUDA thread to compute $\phi_k(\cdot)$ for a specific center. This allows for highly parallel and efficient calculation of kernel values. Similarly, for the optimization phase, the gradient computation is also parallelized by dividing the contributions of different centers across multiple threads. This enables us to efficiently update the transformation parameters during each iteration.

Our CUDA implementation achieves a significant reduction in runtime. The CUDA-accelerated design ensures our moment matching framework can handle point cloud registration with high computational efficiency in real-time applications.

IV. EXPERIMENTS

A. Experimental Setup

In our experiments, we evaluate the performance of the proposed MMR method on both synthetic and real-world datasets. The experiments include two types of setups: pairwise registration experiments on synthetic datasets and SLAM experiments using real-world 4D radar data.

For the pairwise registration experiments, we use the **Stanford Bunny, Dragon, Happy Buddha** and **Armadillo** datasets obtained from the Stanford 3D Scanning Repository [19]. In particular, we choose one point cloud from each of these datasets. To create a registration scenario, we manually apply known rigid transformations to generate a second frame for each point cloud.

For the SLAM experiments, we use the **4D radar dataset** [18] collected in real world. This dataset consists of sparse and noisy data sequences captured by a 4D radar sensor. From this dataset, we integrate our MMR into SLAM to perform registration and evaluate the overall performance.

All experiments are run on an Intel i7-1360P computer with 64GB RAM and a NVIDIA RTX3080Ti GPU.

B. Synthetic experiments for Pairwise Registration

We first evaluate the performance of MMR on noiseless point clouds. Specifically, we select “bun000.ply” from bunny dataset, “dragonStandRight_0.ply” from dragon dataset, “happyStandRight_0.ply” from buddha dataset and “ArmadilloBack_0.ply” from armadillo dataset. In order to satisfy the sparsity requirements for the experiments, the original point clouds are uniformly downsampled to 980, 1078, 791, and 641 points, respectively. Then we manually apply known transformations to create the source and target frames, as shown in Fig. 1. The goal is to recover the applied transformation as accurately as possible.

We evaluate registration performance using two error metrics: the translation error (m) and the rotation error (deg). The errors are computed between the estimated transformation $\hat{\theta}_{M,N}$ and the ground truth transformation θ_0 . In particular,

$$\text{translation error} := \|\text{Trans}(\text{mat}(\theta_0)^{-1} \text{mat}(\hat{\theta}_{M,N}))\|, \quad (6)$$

where $\text{mat}(\theta) := \begin{bmatrix} \mathbf{R} & \mathbf{t} \\ \mathbf{0}^\top & 1 \end{bmatrix}$, and $\text{Trans}(\text{mat}(\theta)) = \mathbf{t}$. In addition,

$$\text{rotation error} := \text{Rot}(\text{mat}(\theta_0)^{-1} \text{mat}(\hat{\theta}_{M,N})), \quad (7)$$

where $\text{Rot}(\text{mat}(\theta)) = \arccos \frac{\text{tr}(\mathbf{R})-1}{2}$ and $\text{tr}(\cdot)$ denotes the trace of a matrix.

We compare the performance of our MMR method against baseline registration methods including NDT and GICP implemented by the Point Cloud Library (PCL) [20]. Table I summarizes the quantitative results.

To further evaluate the robustness of our method, we conduct registration experiments under noisy conditions. For this purpose, to simulate realistic conditions and evaluate the robustness of the proposed method, we introduce two types of artificial noise:

- Gaussian distribution noise: We add random Gaussian noise with standard deviation of 0.005 to the coordinates of the original points, simulating sensor noise.

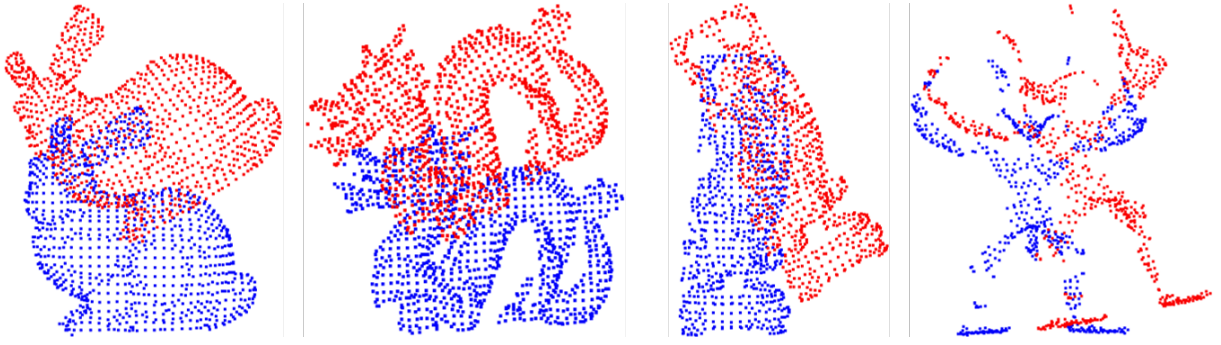


Fig. 1: The source (red) and target (blue) point clouds used for registration in our experiments. From left to right: Bunny, Dragon, Buddha, Armadillo.

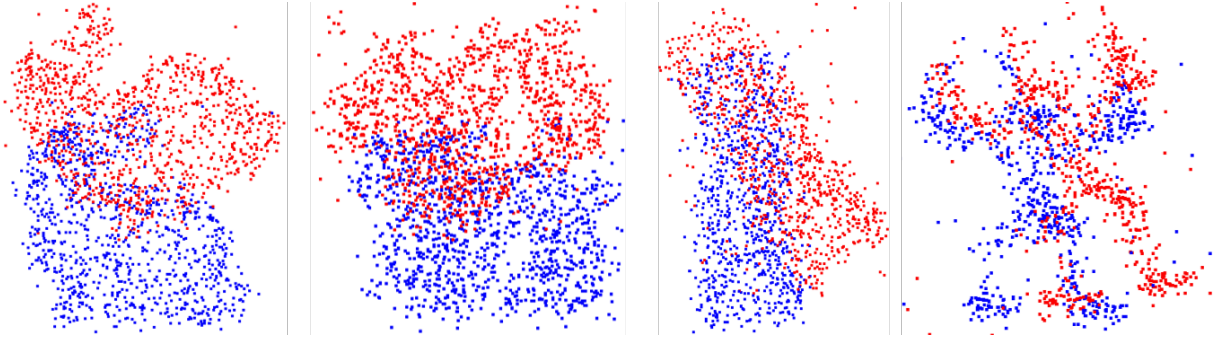


Fig. 2: The noisy source (red) and target (blue) point clouds used for registration in our experiments. From left to right: Noisy Bunny, Noisy Dragon, Noisy Buddha, Noisy Armadillo.

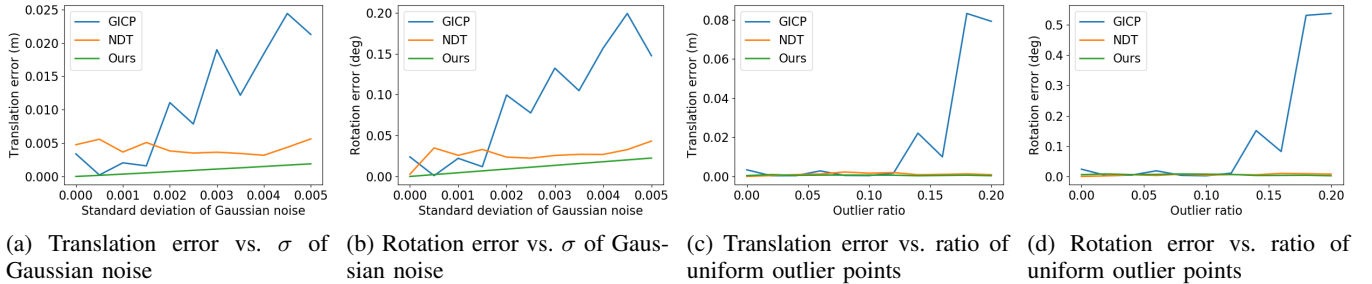


Fig. 3: Comparison of translation and rotation error w.r.t. the standard deviation of Gaussian noise and outlier ratio.

- **Uniform outlier points:** We inject noisy points sampled from a uniform distribution over the spatial extent of the point cloud, imitating environmental clutter. The number of outliers is 10% of the original cloud size.

The noisy point clouds are shown in Fig. 2. Moreover, the registration errors are also computed as in (6) and (7). Table II presents the results, showing the robustness of our method compared to the baselines in the presence of noise.

Moreover, we compare the translation and rotation errors of GICP, NDT, and our proposed method (MMR) under varying levels of Gaussian noise and different ratios of outliers. The results on the Bunny point cloud are presented in Fig. 3. As shown, our method demonstrates superior robustness and stability under heavy noise conditions.

Specifically, GICP is highly sensitive to noise due to its reliance on explicit point correspondences. But the correspondences become unreliable in the presence of noise

and outliers. In contrast, NDT shows improved robustness by leveraging probabilistic surface representations. However, our method consistently outperforms both baselines, particularly under severe noise. Notably, the performance of our method degrades only marginally as the noise level increases, further demonstrating its robustness to noise.

These experiments demonstrate that, in spite of the heavy noise in data, our method achieves more accurate and robust registration performance compared to other point cloud registration methods.

C. Real-world Experiments

To begin with, to demonstrate the practical utility of our method, we implement a scan-to-scan radar odometry using NDT, GICP and MMR and compare their performance on the 4D radar dataset [18]. The use of 4D radar point clouds introduces challenges such as low point density, high noise

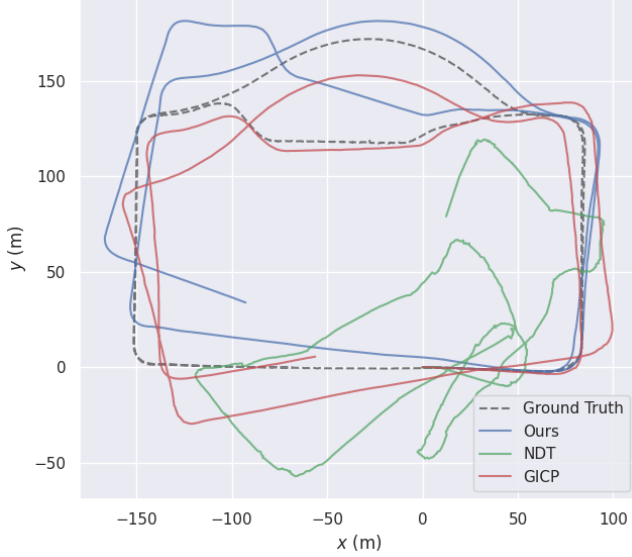


Fig. 4: Comparison of trajectories on data sequence *Campus 1* in 4D radar dataset.

levels, and significant viewpoint changes. The odometry trajectories on the data sequence *Campus 1* are shown in Fig. 4. It shows that NDT fails to estimate transformations because of the sparsity of 4D radar point clouds. Moreover, to further compare the performance of GICP and MMR, we further compute the relative error (RE) following the KITTI odometry benchmark [21]. In particular, we compute the mean translation and rotation errors from length 100 m to 800 m with a 100 m increment. Translation errors are in percentage (%), and rotation errors are in degrees per meter (deg/m). Consequently, our method achieves superior RE (3.69% / 0.0245 deg/m) compared to GICP (4.18% / 0.0251 deg/m). Nevertheless, our MMR requires approximately 158 ms per frame for registration. It indicates that the algorithm's real-time capability still needs further improvement.

Next, we integrate MMR into the 4DRaSLAM framework [18] to evaluate the performance in a complete SLAM system. In particular, we replace the scan-to-submap NDT-based registration with our scan-to-submap MMR in the Scan Registration module. Unlike pairwise registration, this experiment registers consecutive frames to submaps to build a globally consistent map. Therefore, besides RE, we also include the root-mean-square error (RMSE) of absolute trajectory error (ATE) in meters (m) to evaluate the global consistency of the estimated trajectory [22]. The results are listed in Table III in the format of "translation error (%) / rotation error (deg/m) / ATE (m)". The results show that our method effectively handles the sparsity and noise issues of 4D radar points and achieves accurate and robust pose estimation comparable to LiDAR-based SLAM [16], [17].

V. CONCLUSIONS

In this work, we introduced a moment matching-based point cloud registration method. Our approach uses Gaussian

radial basis function kernels to compute the moments of point cloud. It captures the global structure of the point clouds and avoids reliance on point correspondences. The experiments demonstrate that our method consistently achieves better accuracy and stability compared to other registration approaches. We further integrated this framework into a 4D radar-based SLAM system. The results show that our MMR improves localization performance to levels similar to LiDAR-based SLAM.

In future work, we aim to further enhance the real-time performance of the algorithm. Moreover, we will extend the framework to support non-rigid transformations. These improvements will broaden the applicability of our method to more dynamic and complex environments.

APPENDIX

Lemma 1: Let $\Phi(\mathbf{x}) := [\phi_1(\mathbf{x}), \phi_2(\mathbf{x}), \dots, \phi_\kappa(\mathbf{x})]^\top$ be a κ -dimensional vector-valued kernel function where ϕ_k 's are defined as (3). If the centers $\{\mathbf{c}_k\}_{k=1}^\kappa$ do not lie in any hyperplane in \mathbb{R}^3 , then Φ is injective.

Proof: We use contradiction proof. Assume $\exists \mathbf{x}_1 \neq \mathbf{x}_2$ such that $\Phi(\mathbf{x}_1) = \Phi(\mathbf{x}_2)$. This implies $\|\mathbf{x}_1 - \mathbf{c}_k\|_{\Sigma^{-1}}^2 = \|\mathbf{x}_2 - \mathbf{c}_k\|_{\Sigma^{-1}}^2$ holds for $k = 1, \dots, \kappa$. And it follows that $2\Delta\mathbf{x}^\top \Sigma^{-1}(\mathbf{x}_2 - \mathbf{c}_k) + \Delta\mathbf{x}^\top \Sigma^{-1} \Delta\mathbf{x} = 0$ for all $k = 1, \dots, \kappa$. This implies $\mathbf{b}^\top \mathbf{c}_k = \text{constant}$ for all $k = 1, \dots, \kappa$, where $\mathbf{b} = \Sigma^{-1} \Delta\mathbf{x}$ is a nonzero constant vector. Hence \mathbf{c}_k lives in a hyperplane, which contradicts the assumption. ■

Proof: (Proof of Theorem 1) Let $z_1 \sim \text{Bernoulli}\left(\frac{N}{N+M}\right)$ be a binary random variable indicating whether a sample is drawn from the source or target distribution. Let $\mathbf{z}_2 \in \mathbb{R}^3$ be a spatial point such that $\mathbf{z}_2 \sim \mu \circ T_0$ when $z_1 = 0$, and $\mathbf{z}_2 \sim \mu$ when $z_1 = 1$. Further denote $\mathbf{z} := [z_1, \mathbf{z}_2^\top]^\top$. Furthermore, let $\mathbf{g}: \mathbb{R}^4 \times \text{SE}(3) \rightarrow \mathbb{R}^\kappa$ be

$$\mathbf{g}(\mathbf{z}; \theta) = (1 - z_1) \cdot \Phi(\mathbf{R}\mathbf{z}_2 + \mathbf{t}) \cdot \frac{N + M}{N} - z_1 \cdot \Phi(\mathbf{z}_2) \cdot \frac{N + M}{M}.$$

Next, take expectation of the above function with respect to \mathbf{z} , we get

$$\begin{aligned} \mathbb{E}[\mathbf{g}(\mathbf{z}; \theta)] &= \frac{N + M}{N} \mathbb{E}[\Phi(\mathbf{R}\mathbf{z}_2 + \mathbf{t}) | z_1 = 0] \cdot \underbrace{\mathbb{P}(z_1 = 0)}_{\frac{N}{N+M}} \\ &\quad + \frac{N + M}{N} \mathbb{E}[\Phi(\mathbf{R}\mathbf{z}_2 + \mathbf{t}) | z_1 = 1] \cdot 0 \cdot \mathbb{P}(z_1 = 1) \\ &\quad - \frac{N + M}{M} \mathbb{E}[\Phi(\mathbf{z}_2) | z_1 = 0] \cdot 0 \cdot \mathbb{P}(z_1 = 0) \\ &\quad - \frac{N + M}{M} \mathbb{E}[\Phi(\mathbf{z}_2) | z_1 = 1] \underbrace{\mathbb{P}(z_1 = 0)}_{\frac{N+M}{M}} \\ &= \mathbb{E}_{\mu \circ T_0}[\Phi(T(\mathbf{x}; \theta))] - \mathbb{E}_\mu[\Phi(\mathbf{y})]. \end{aligned}$$

Consequently, the "original" objective function $\mathcal{L}(\theta)$ in (4) that we are minimizing can be rewritten into the following compact form $\mathcal{L}(\theta) = \|\mathbb{E}[\mathbf{g}(\mathbf{z}; \theta)]\|^2$. This falls exactly into the scope of Generalized Method of Moment (GMM) [23], where we approximate the expectation with empirical mean.

Hence we can prove the consistency by checking whether the consistency conditions for GMM are satisfied. In particular,

- The parameter domain $\theta \in \mathcal{B}(\eta)$ is compact. Recall the definition of $\theta \in \mathcal{B}(\eta)$, the space $\text{SO}(3)$ for rotation matrix \mathbf{R} is clearly compact. Moreover, we force $\|\mathbf{t}\|^2 \leq \eta$ in $\theta \in \mathcal{B}(\eta)$ because in practice the translation is often bounded to a known range, and hence the statement follows.
- $\mathbf{g}(\mathbf{z}; \theta)$ is continuous at each θ with probability one. This holds from the fact that the kernel function Φ is continuous, and the transformation $T(\cdot; \theta)$ acts continuously on $\mathbf{z}_2 \in \mathbb{R}^3$. Therefore, for every realization of \mathbf{z} , the mapping $T \mapsto \mathbf{g}(\mathbf{z}; \theta)$ is continuous.
- $\mathbb{E}[\sup_{\theta \in \mathcal{B}(\eta)} \|g(\mathbf{z}; \theta)\|] < \infty$. This holds from the fact that the kernel function Φ is bounded. Specifically, since Φ consists of K Gaussian radial basis functions, each satisfying $0 < \phi_k(\mathbf{x}) \leq 1$. Hence $\|\Phi(\mathbf{x})\| \leq \sqrt{K}$. In addition, z_1 is either 0 or 1 since it is Bernoulli distributed. These together gives the statement.
- $\mathbb{E}[\mathbf{g}(\mathbf{z}; \theta)] = 0$ has a unique solution θ_0 . Let $\mathbb{E}[\mathbf{g}(\mathbf{z}; \theta)] = 0$ and this implies

$$\mathbb{E}[\mathbf{g}(\mathbf{z}; \theta)] = \mathbb{E}_{\mu \circ T_0}[\Phi(T(\mathbf{x}; \theta))] - \mathbb{E}_{\mu}[\Phi(\mathbf{y})] = 0.$$

On the other hand, by the definition of $\mu \circ T_0$, we can write $\mathbb{E}_{\mu \circ T_0}[\Phi(T(\mathbf{x}; \theta))]$ as

$$\begin{aligned} \mathbb{E}_{\mu \circ T_0}[\Phi(T(\mathbf{x}; \theta))] &= \int_{T_0^{-1}(\mathbb{K})} \Phi(T(\mathbf{x}; \theta)) (\mu \circ T_0)(d\mathbf{x}) \\ &= \int_{\mathbb{K}} \Phi(T(T_0^{-1}(\mathbf{y}); \theta)) \mu(d\mathbf{y}), \end{aligned}$$

which further equals to $\mathbb{E}_{\mu}[\Phi(\mathbf{y})] = \int_{\mathbb{K}} \Phi(\mathbf{y}) \mu(d\mathbf{y})$. This implies $\Phi(T(T_0^{-1}(\cdot); \theta)) = \Phi(\cdot)$, μ -a.s.. By Lemma 1, this further implies $T_{\theta} \circ T_0^{-1} = \text{Id}$ and hence $\theta = \theta_0$.

Therefore, all of the consistency conditions for GMM are satisfied and we have $\hat{\theta}_{M,N} \xrightarrow{P} \theta_0$ as $M, N \rightarrow \infty$. ■

REFERENCES

- [1] X. Huang, G. Mei, J. Zhang, and R. Abbas, “A comprehensive survey on point cloud registration,” *arXiv preprint arXiv:2103.02690*, 2021.
- [2] P. J. Besl and N. D. McKay, “Method for registration of 3-d shapes,” in *Sensor fusion IV: control paradigms and data structures*, vol. 1611. Spie, 1992, pp. 586–606.
- [3] P. Biber and W. Straßer, “The normal distributions transform: A new approach to laser scan matching,” in *Proceedings 2003 IEEE/RSJ International Conference on Intelligent Robots and Systems (IROS 2003)(Cat. No. 03CH37453)*, vol. 3. IEEE, 2003, pp. 2743–2748.
- [4] M. Magnusson, “The three-dimensional normal-distributions transform: an efficient representation for registration, surface analysis, and loop detection,” Ph.D. dissertation, Örebro universitet, 2009.
- [5] S. Zhang, A. Ringh, X. Hu, and J. Karlsson, “Modeling collective behaviors: A moment-based approach,” *IEEE Transactions on Automatic Control*, vol. 66, no. 1, pp. 33–48, 2020.
- [6] A. Segal, D. Haehnel, and S. Thrun, “Generalized-icp,” in *Robotics: science and systems*, vol. 2, no. 4. Seattle, WA, 2009, p. 435.
- [7] K. Koide, M. Yokozuka, S. Oishi, and A. Banno, “Voxelized gicp for fast and accurate 3d point cloud registration,” in *2021 IEEE International Conference on Robotics and Automation (ICRA)*. IEEE, 2021, pp. 11 054–11 059.
- [8] R. B. Rusu, N. Blodow, and M. Beetz, “Fast point feature histograms (fpfh) for 3d registration,” in *2009 IEEE international conference on robotics and automation*. IEEE, 2009, pp. 3212–3217.
- [9] S. Salti, F. Tombari, and L. Di Stefano, “Shot: Unique signatures of histograms for surface and texture description,” *Computer vision and image understanding*, vol. 125, pp. 251–264, 2014.
- [10] Y. Wang and J. M. Solomon, “Deep closest point: Learning representations for point cloud registration,” in *Proceedings of the IEEE/CVF international conference on computer vision*, 2019, pp. 3523–3532.
- [11] Y. Aoki, H. Goforth, R. A. Srivatsan, and S. Lucey, “Pointnetlk: Robust & efficient point cloud registration using pointnet,” in *Proceedings of the IEEE/CVF conference on computer vision and pattern recognition*, 2019, pp. 7163–7172.
- [12] C. R. Qi, H. Su, K. Mo, and L. J. Guibas, “Pointnet: Deep learning on point sets for 3d classification and segmentation,” in *Proceedings of the IEEE conference on computer vision and pattern recognition*, 2017, pp. 652–660.
- [13] X. Li, J. K. Pontes, and S. Lucey, “Pointnetlk revisited,” in *Proceedings of the IEEE/CVF conference on computer vision and pattern recognition*, 2021, pp. 12 763–12 772.
- [14] J. E. Dennis, Jr and J. J. Moré, “Quasi-newton methods, motivation and theory,” *SIAM review*, vol. 19, no. 1, pp. 46–89, 1977.
- [15] J. D. Head and M. C. Zerner, “A broyden—fletcher—goldfarb—shanno optimization procedure for molecular geometries,” *Chemical physics letters*, vol. 122, no. 3, pp. 264–270, 1985.
- [16] G. Kim and A. Kim, “Scan Context: Egocentric Spatial Descriptor for Place Recognition Within 3D Point Cloud Map,” in *2018 IEEE/RSJ International Conference on Intelligent Robots and Systems (IROS)*, Oct. 2018, pp. 4802–4809, iSSN: 2153-0866.
- [17] T. Shan and B. Englot, “Lego-loam: Lightweight and ground-optimized lidar odometry and mapping on variable terrain,” in *2018 IEEE/RSJ international conference on intelligent robots and systems (IROS)*. IEEE, 2018, pp. 4758–4765.
- [18] X. Li, H. Zhang, and W. Chen, “4d radar-based pose graph slam with ego-velocity pre-integration factor,” *IEEE Robotics and Automation Letters*, vol. 8, no. 8, pp. 5124–5131, 2023.
- [19] B. Curless and M. Levoy, “A volumetric method for building complex models from range images,” in *Proceedings of the 23rd annual conference on Computer graphics and interactive techniques*, 1996, pp. 303–312.
- [20] R. B. Rusu and S. Cousins, “3d is here: Point cloud library (pcl),” in *2011 IEEE international conference on robotics and automation*. IEEE, 2011, pp. 1–4.
- [21] A. Geiger, P. Lenz, and R. Urtasun, “Are we ready for autonomous driving? The KITTI vision benchmark suite,” in *2012 IEEE Conference on Computer Vision and Pattern Recognition*, Jun. 2012, pp. 3354–3361, iSSN: 1063-6919.
- [22] J. Sturm, N. Engelhard, F. Endres, W. Burgard, and D. Cremers, “A benchmark for the evaluation of rgb-d slam systems,” in *2012 IEEE/RSJ international conference on intelligent robots and systems*. IEEE, 2012, pp. 573–580.
- [23] L. P. Hansen, “Large sample properties of generalized method of moments estimators,” *Econometrica: Journal of the econometric society*, pp. 1029–1054, 1982.